



## Article

# Laser-Plasma Spectroscopy of Hydroxyl with Applications

Christian G. Parigger<sup>1,\*</sup> , Christopher M. Helstern<sup>1</sup>, Benjamin S. Jordan<sup>2</sup>, David M. Surmick<sup>3</sup> , Robert Splinter<sup>4</sup>

<sup>1</sup> Physics and Astronomy Department, University of Tennessee, University of Tennessee Space Institute, Center for Laser Applications, 411 B.H. Goethert Parkway, Tullahoma, TN 37388-9700, USA; chris.helstern@gmail.com

<sup>2</sup> Nuclear Engineering Department, University of Tennessee, Tickle College of Engineering, 1412 Circle Drive, Knoxville, TN 37912, USA; bjordan1@vols.utk.edu

<sup>3</sup> Physics and Applied Physics Department, University of Massachusetts Lowell, Lowell, MA 01854, USA; David\_Surmick@uml.edu

<sup>4</sup> Welling Medical, Van der Waals Park 22, 9351 VC Leek, The Netherlands; rsplinter@gmail.com

\* Correspondence: cparigge@tennessee.edu; Tel.: +1 (931)-841-5690

**Abstract:** This article discusses laser-induced laboratory-air plasma measurements and analysis of hydroxyl (OH) ultraviolet spectra. New experiments with Q-switched laser pulses illustrate occurrence of molecular recombination spectra for time delays of the order of several dozen of microseconds after plasma initiation. The computation of the emission spectra utilizes line strength data that are communicated as a supplementary file. Applications of detailed OH computations include laser-induced plasma and combustion analyses, to name but two applications.

**Keywords:** plasma diagnostics; molecular spectra; diatomic molecules; plasma spectroscopy; laser spectroscopy; laser-induced breakdown spectroscopy; optical emission spectroscopy; molecular excitation temperature; combustion analysis, astrophysical spectroscopy

## 1. Introduction

Practical applications of molecular spectroscopy include diagnosis of hydroxyl (OH) diatomic molecules in the study of laboratory plasma and chemical processes. Laser spectroscopy [1–3] usually delivers information about the temporal- and spatial- distribution of species. Diagnosis usually utilizes methods that are frequently encountered in characterization of plasma [4]. This work communicates aspects of laser spectroscopy of OH that include active interrogation with excitation from ground- or lower molecular states and levels, viz. laser-induced fluorescence (LIF), and passive analyses of excited molecular states or levels encoded in the emitted light from laser-induced plasma, viz. optical emission spectroscopy (OES). However, laser spectroscopy examples primarily focus on OES of the OH molecule and at standard ambient temperature and pressure (SATP) laboratory conditions.

Molecular recombination spectra are readily observed following optical breakdown in laboratory air. Emission signals from the OH molecule in the UV near 306 nm can be recognized in air breakdown for time delays of the order of 10  $\mu$ s after cessation of the laser pulse, but recorded data for the  $\Delta v = 0$  OH bands indicate spectral interference with N<sub>2</sub> second positive bands [5,6]. For time delays of the order of 100  $\mu$ s, however, ultraviolet OH emissions of the  $\Delta v = 0$  bands dominate in the range of 305 nm to 322 nm. Hydrocarbon combustion typically produces OH that can be measured with laser-induced fluorescence (LIF) and planar laser-induced fluorescence [7,8].

This work aims to (a) publish OH line strength data [9] that can be directly utilized with associated graphing and non-linear fitting programs [10] that include the Nelder-Mead temperature (NMT) program and the Boltzmann equilibrium spectroscopy program (BESP); (b) communicate new experimental investigations for the purpose of estimating both typical signal strength and time-delays for occurrence of hydroxyl spectra in laboratory laser-sparks; (c) summarize possible approaches for determination of OH concentrations with reference to local equilibrium conditions for a variety of plasma species; (d) illustrate typical fluid physics phenomena that can be initially explored by employing shadowgraph techniques; (e) comment on the set extensively LIF- and OES- tested OH line strength data with respect to alternate or perhaps historic approaches for computation of theory spectra, and (f) stimulate further fundamental analysis and comparisons with laboratory data.

Fundamental analysis includes investigations of differences in spectra for OH and OD isotopologues using the program LIFBASE [11]. Applications include laser ablation molecular isotopic spectrometry (LAMIS) [12]. Recent OH data-base developments [13] for predictions with PGOPHER [14] indicate the continued interest in establishing well-defined parameters for prediction of OH spectra. This work facilitates transition towards analysis of diatomic molecules, viz. hydroxyl, abundant in interstellar medium (ISM) along with other matter and radiation in the region between star systems. In this work, including exo-planet studies, the ExoMol data-base [16,17] is expected to assist in analysis of available superposition spectra.

## 2. Mini summary of OH literature

The OH diatomic molecule occurs frequently as an intermittent molecule as part of a volley of chemical reactions that occur for example in plasma and that are measured in combustion processes. Examples of fundamental interests include exploration of the effects of chemical reactions on non-isothermal plasma [17] and the effect of N<sub>2</sub> and O<sub>2</sub> on OH production [18]. Related studies focus on line-by-line emission spectra from non-equilibrium plasma [19]. Moreover, as another example, the OH radical has been employed for velocity mapping [20].

The literature on OH spectroscopy is rather exhaustive, and this work only communicates a subset of papers that are of interest in hydroxyl diagnosis. Spectroscopic data for OH analysis are typically derived from Fourier transform spectroscopy [20,21] or by detailed studies of rotational spectra [22]. Fundamental data of OH molecular transitions are communicated in selected References [24–42]. Interrogations of ground-state or ground-level populations employ laser-induced fluorescence [43–63] with practical applications to combustion diagnosis [64–71]. LIF and the specific example of combustion analysis however are based on extensive studies of the ultraviolet OH system [72–90].

## 3. Experimental details

Standard experimental components are used for laser-induced breakdown spectroscopy, summarized previously, but are included for completeness, e.g., see Ref. [91] or for general laser-induced breakdown spectroscopy Refs. [92,93]. The arrangement for the experiments reported in this work consists of a set of components typical for time-resolved, laser-induced optical emission spectroscopy, or nanosecond laser-induced breakdown spectroscopy (LIBS) [92]. Primary instrumentation includes a Q-switched neodymium-doped yttrium aluminum garnet, Nd:Y<sub>3</sub>Al<sub>5</sub>O<sub>12</sub> (Nd:YAG) device (Quantel model Q-smart 850, USA) operated at the fundamental wavelength of 1064-nm to produce full-width-at-half-maximum 6-ns laser radiation with an energy of up to 850 mJ per pulse, a laboratory type Czerny-Turner spectrometer (Jobin Yvon model HR 640, Fr) with a 0.64-m focal length and equipped with a 1200 grooves/mm grating, an intensified charge coupled device (Andor Technology model iStar DH334T-25U-03, USA) for recording of temporally and spatially resolved spectral data, electronic components for synchronization, and various optical elements for beam shaping, steering and focusing.

In previous experiments, captured shadowgraphs of the breakdown plasma [94] served the purpose of visualizing the plasma expansion when using 850 mJ, 6-ns radiation. The captured images

are consistent with results of fluid-dynamic expansion phenomena [95] presented in the literature. In laser-ablation research, shockwave expansion studies [96] from a solid sample into air or a into a gaseous environment such as argon are important for laser-induced breakdown spectroscopy (LIBS) that is applied for determination of elemental composition of the sample.

However, it is important to obtain shadowgraphs for plasma excitation energies that were employed for time-resolved spectroscopy. Shadowgraphs reported recently [91] are captured using two separate laser devices (Continuum Surelite model SL I-10, USA) that can be externally operated to deliver laser pulses with a well-defined time delay showing less than  $\pm 1$  ns trigger-jitter between the pulses. The experiments reported in Ref. [91] are extended to time delays of the order of 100  $\mu$ s for the purpose of visualizing the breakdown site for time delays that correspond to reasonable OH signals.

For visualization studies, both lasers are frequency-doubled to operate at the 2<sup>nd</sup> harmonic, 532-nm wavelength, and both beams are spatially overlapped. Both pulses can be delivered with a minimum time delay of 300 ns. Shadowgraphs are recorded by external synchronization of the Surelite and Quantel laser devices and by externally triggering the camera (Silicon Video 9C10 color camera, USA) that records the images that are projected onto a screen.

## 4. Results and discussion

### 4.1. Shadowgraphs

Figures 1a and 1b illustrate typical shadowgraphs recorded for time-delays of 54.25  $\mu$ s and 104.25  $\mu$ s, respectively. The laser is incident from the right as indicated by the arrow in the single shot captured shadowgraph. While an outgoing shockwave occurs for time delays of the order of 1  $\mu$ s, as recently communicated in Ref. [91], Fig. 1 depicts well developed vortices and fluid flow towards the incoming laser beam. In view of laser spectroscopy, a time-resolved data taken along a narrow slice along the horizontal direction would be affected by fluid dynamics.

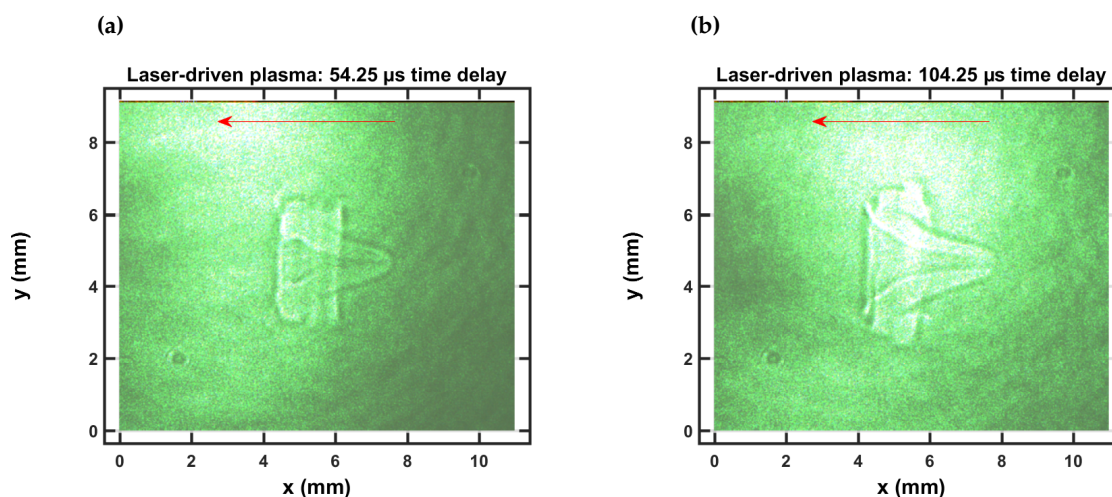


**Figure 1.** Single-shot shadowgraph of the expanding laser-induced plasma initiated with a 170-mJ, 6-ns, 1064-nm focused beam, and imaged using a 5-ns, 532-nm back-light that is time-delayed by (a) 54.25  $\mu$ s and (b) 104.25  $\mu$ s.

### 4.2. Measurement of OH spectra

Time-resolved spectroscopy of laser-induced plasma in laboratory air at a humidity level of 25% reveal characteristic uv OH data due to molecular recombination. Optical breakdown was generated at a rate of 10 Hz, with the laser beam focused with f/5 optics from the top, or parallel to the slit, analogous to recently reported CN laser spectroscopy [91]. The detector pixels are binned in 4-pixel tracks along the slit direction, resulting in obtaining 256 spectra for each time delay. Measurements

comprise accumulation of 100 consecutive laser-plasma events for 11 separate time delays at  $10\ \mu\text{s}$  steps. The selected series explores the plasma decay with specific attention to recognition of OH molecular data free from spectroscopic interference. Figures 2 and 3 illustrate spatio-temporal spectra that were recorded along the line-of-sight. The slit-height corresponds to the x-direction in Fig. 1 and the line-of-sight corresponds to direction of the back light used for capture of shadowgraphs.

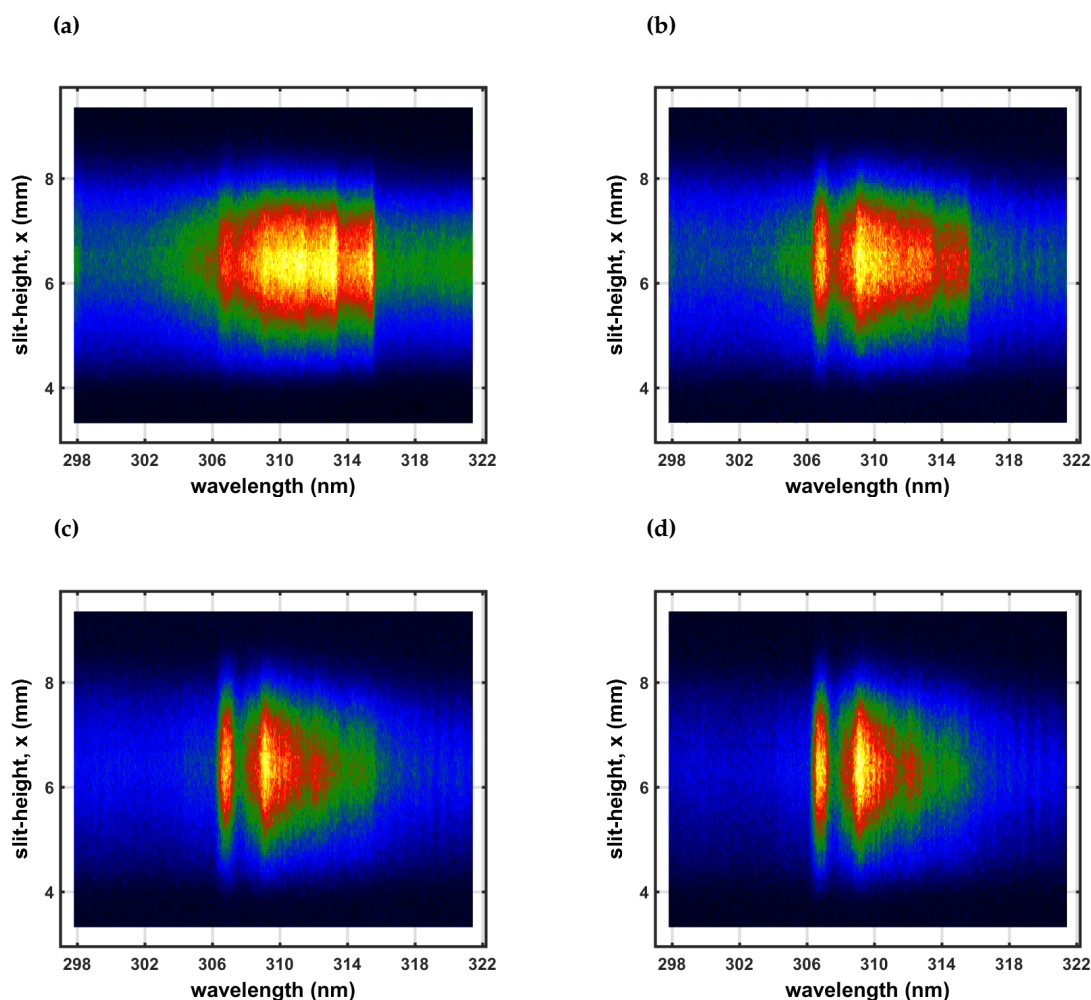


**Figure 2.** Recorded data of slit-height vs. wavelength. Gate width:  $10\ \mu\text{s}$ , time delay (a)  $20\ \mu\text{s}$  – primarily  $\text{N}_2$  second positive spectra, (b)  $30\ \mu\text{s}$ , (c)  $40\ \mu\text{s}$ , and (d)  $50\ \mu\text{s}$  – primarily OH spectra.

The raw spectra in Figure 2 and the corresponding averages in 3 are consistent with previously recorded spectra using a UV-enhanced, intensified linear-diode array [5,97]. Early delay-time data were analyzed using classic laser spectroscopy, namely, addition of superimposed  $\text{N}_2$  second positive and OH spectra. Moreover, a program designed for study of plasma torches was applied using chemical equilibrium. It is clear that a variety of species, including electrons, contribute to the measured spectra [5,6]. Investigations of information content and error propagation analysis reveals reasonable diagnosis capabilities of the line-of-sight analysis.



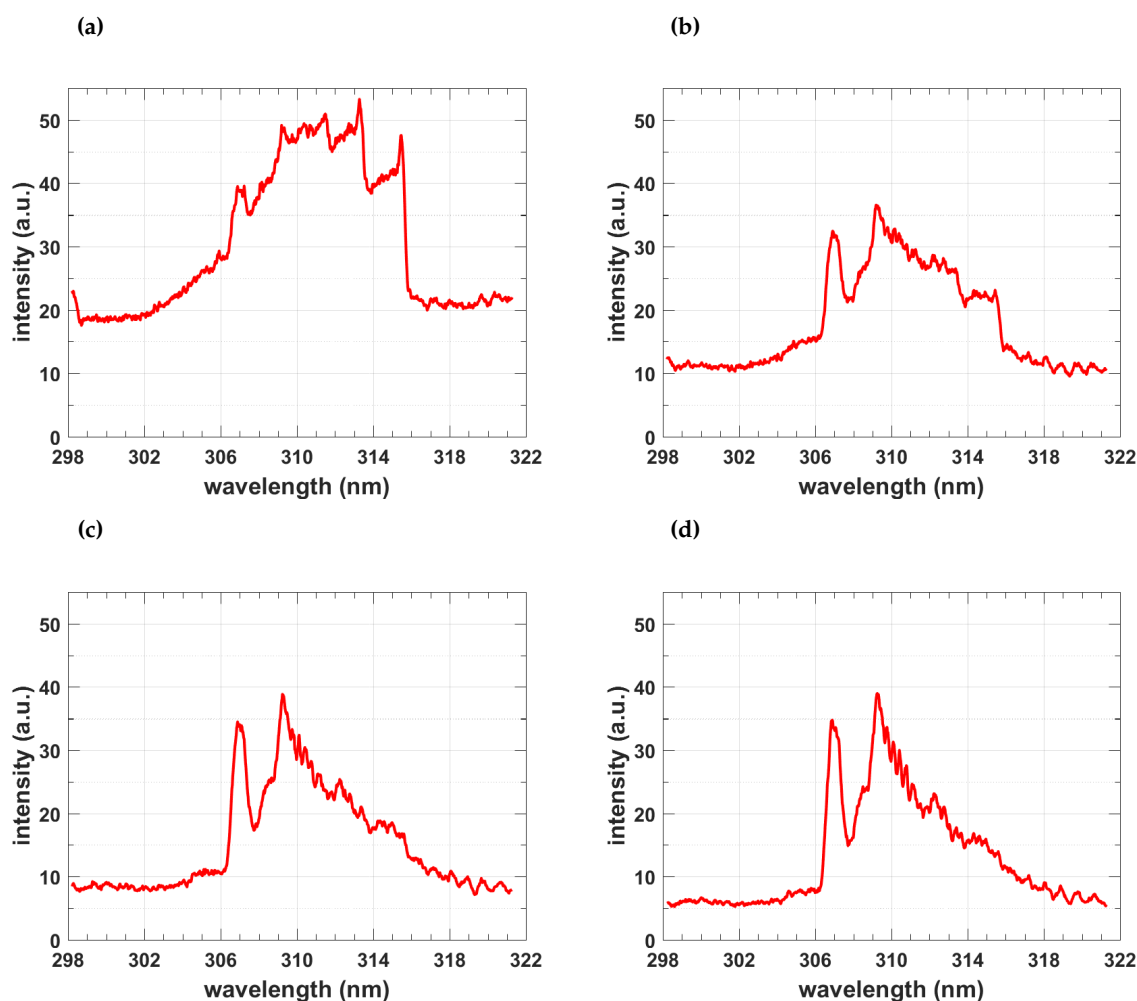


**Figure 3.** Average of spectra between 4.2 and 8.2 mm of Figure 2. Gate width: 10  $\mu$ s, time delay (a) 20  $\mu$ s – primarily N<sub>2</sub> second positive spectra (b) 30  $\mu$ s, (c) 40  $\mu$ s, and (d) 50  $\mu$ s – primarily OH spectra. Contributions from the N<sub>2</sub> second positive system diminish with increase of time delays.

In view of the recorded shadowgraphs (see Fig. 1), there appears to be well defined fluid physics phenomena including vortex formation and implosion of the shockwave-dominated expansions. The vortex is well developed and the implosion towards the laser device is recognizable in Fig. 1 for time delays of approx. 50 and 100  $\mu$ s. The direction of the implosion is determined by slightly asymmetric energy absorption, in other words, by the direction of the laser-beam. The energy absorption causes slight asymmetries of shock waves for pulse energies of 160 to 200 mJ/pulse [5], and the expansion speeds are above hypersonic for time delays of approx. 0.5  $\mu$ s.

Table 1 conveys the shockwave radii for laser-induced plasma initiated with energies 200 mJ/pulse in standard ambient temperature and pressure (SATP) air. The table entries confirm that for 200-mJ/pulse the shockwave is outside the vertical dimension of the available slit of approx. 14-mm height for 1:1 imaging. The shockwave radii were calculated using Taylor-Sedov model, analogous to recently published investigation of CN spectra [46],

$$R(\tau) = \left( \frac{E}{\rho} \tau^2 \right)^{1/5}. \quad (1)$$

The shockwave radius,  $R(\tau)$ , is a function of absorbed pulse energy,  $E$ , density of the gas,  $\rho$ , and time delay,  $\tau$ .

**Table 1.** Computed shockwave radii for SATP air, 200 mJ energy/pulse.

time delay ( $\mu$ s)	$R(\text{mm})$ for air [ $\rho = 1.2 \text{ kg/m}^3$ ]
20	9.21
25	10.1
50	13.3
75	15.7
100	17.5

4.3. Computation of OH spectra

The computation of OH diatomic molecular spectra is based on collection of line-strength data [9] and application of algorithms for comparison of measured and computed spectra [10]. Figure 4 illustrates computed OH data for spectral resolutions of 0.25 nm and 0.0025 nm that correspond to typical resolutions in laser-induced spectroscopy with intensified array detectors and nominal pico-meter resolution stick-spectra. The line-strength data are included as a supplement, and Appendix A reports typical fitting results of well-calibrated data [5] in terms of wavelength and instrument sensitivity.

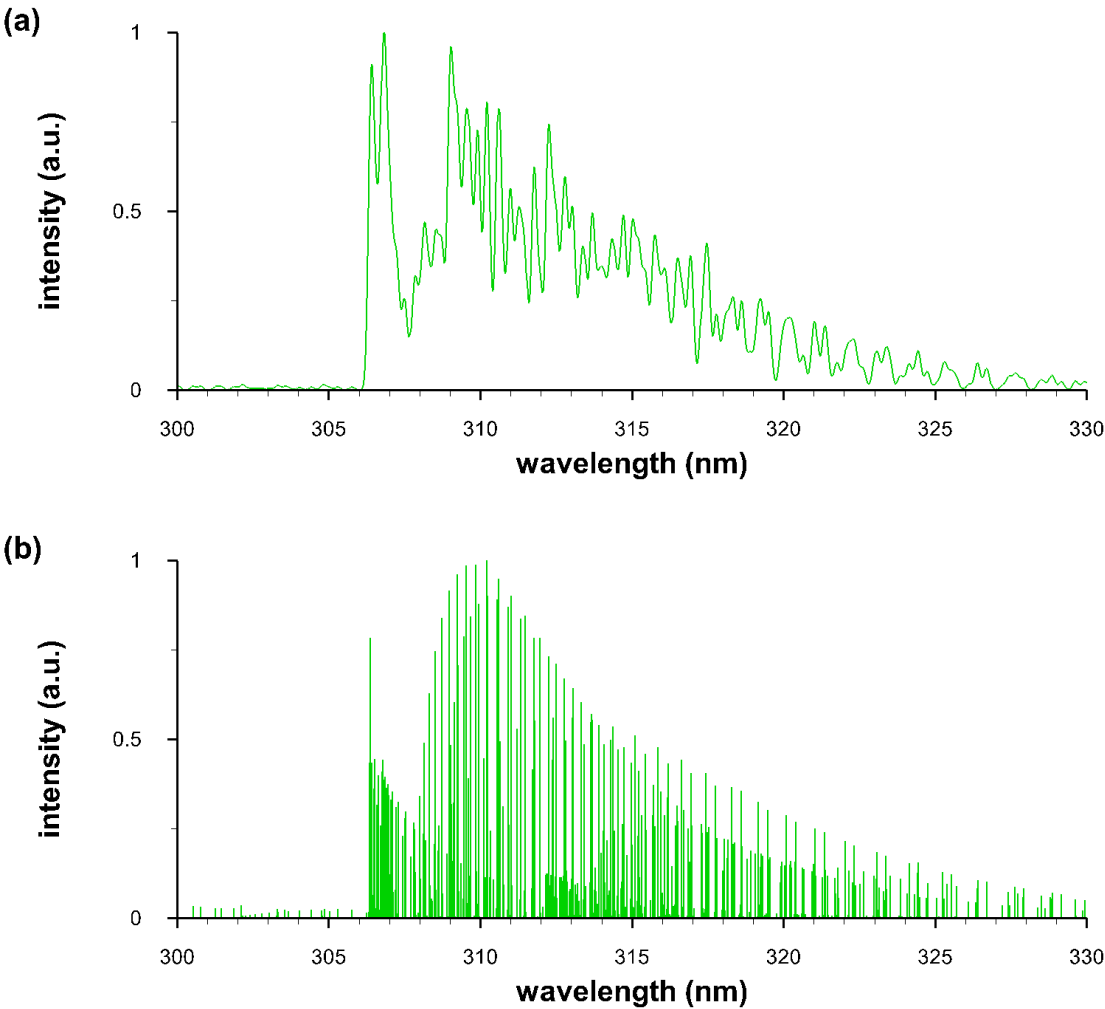


**Figure 4.** Computed spectra: T = 6,000 K; Spectral resolution (a) 0.25 nm and (b) 0.0025 nm.

#### 4.4. Comparisons of recorded and computed OH spectra

The accuracy of the line strength data can be evaluated by comparing predictions with optical emission spectroscopy (OES) and laser induced fluorescence (LIF) records. Line strength wavelengths are accurate to better than  $0.05\text{ cm}^{-1}$  or better than  $0.5\text{ pm}$  at a wavelength of  $300\text{ nm}$ . In passive emission spectroscopy, small variations in the precision of the computed spectral data can add up to differences in predicted and measured data although laser-plasma spectral resolutions are frequently of the order of  $0.1\text{ nm}$ , in other words, the line strength wavelengths are known about a factor of 200 better than available in OES. In addition, the predicted relative magnitudes of individual lines within a band system need to agree as well.

The hydroxyl  $A^2\Sigma^+ \leftrightarrow X^2\Pi_i$  ultraviolet system line strengths (see Appendix A) contain 0-0, 0-1, 1-0, 1-1, 1-2, 2-0, 2-1, 2-2, and 2-3 bands. Centrifugal stretching of the Franck-Condon factors and r-centroids are included in the process of determining the line strengths. Figures 5 and 6 illustrate laser induced fluorescence and optical emission spectroscopy comparisons. Fig. 6 also shows contributions from the different bands of the  $\Delta v = 0$  OH transitions.

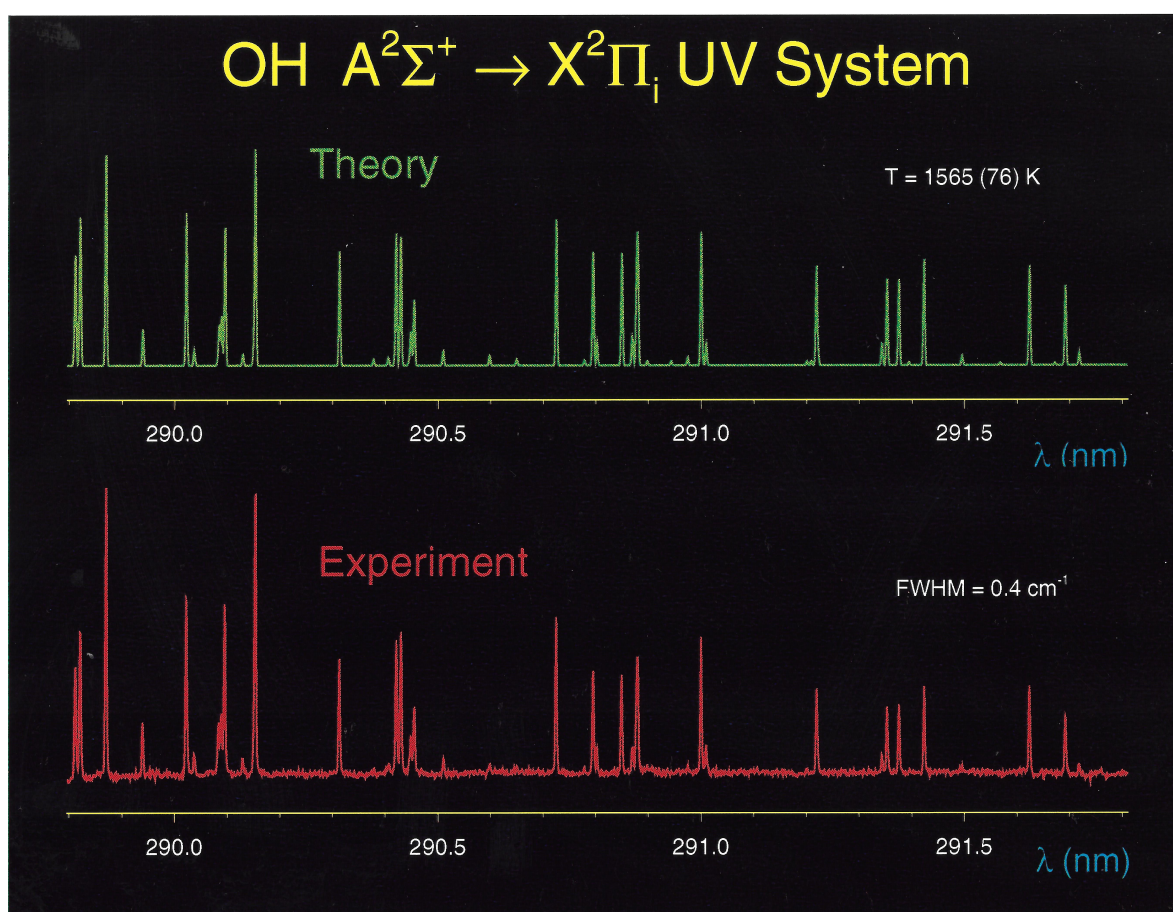


**Figure 5.** Comparisons of measured and recorded laser induced fluorescence spectra [99].

#### 4.5. Temperature and density of OH

The temperature is inferred from the OH spectra by fitting measured with computed molecular spectra. The procedure, program and a example result are included in the Appendix A. In this work, an average temperature is obtained from the line-of-sight data assuming an equilibrium plasma excitation temperature. This particular assumption has been investigated by employing predictions from chemical equilibrium codes as input to a general non-equilibrium air radiation program [5,6]. Various species densities are predicted within the equilibrium assumption, and include OH, Ar, N, O,  $e^-$ ,  $N_2$ ,  $O_2$ , CO, NO,  $NO^+$  (see Table 1 in Reference [5]). For laboratory air, the OH concentration

maximum occurs at temperatures of approx. 3,000 K at a time delay of approx. 100  $\mu$ s and are of the order of  $10^{16}$  cm $^{-3}$ . A detailed study [5] used linear diode arrays and employed up to 100 Hz repetition rate from a Nd:YAG laser device (Coherent Infinity 40-100, USA). Determination of OH temperature and molecular species concentrations in laser-induced laboratory air breakdown includes Monte Carlo simulation as well for estimation of error bars [5]. Contributions from species other than OH for time delays of the order of 100  $\mu$ s can be calculated using a general non-equilibrium program in the equilibrium mode, with inputs obtained from chemical equilibrium codes - one finds approx. 5% wavelength-dependent peak-background contributions from species other than OH [98,99].

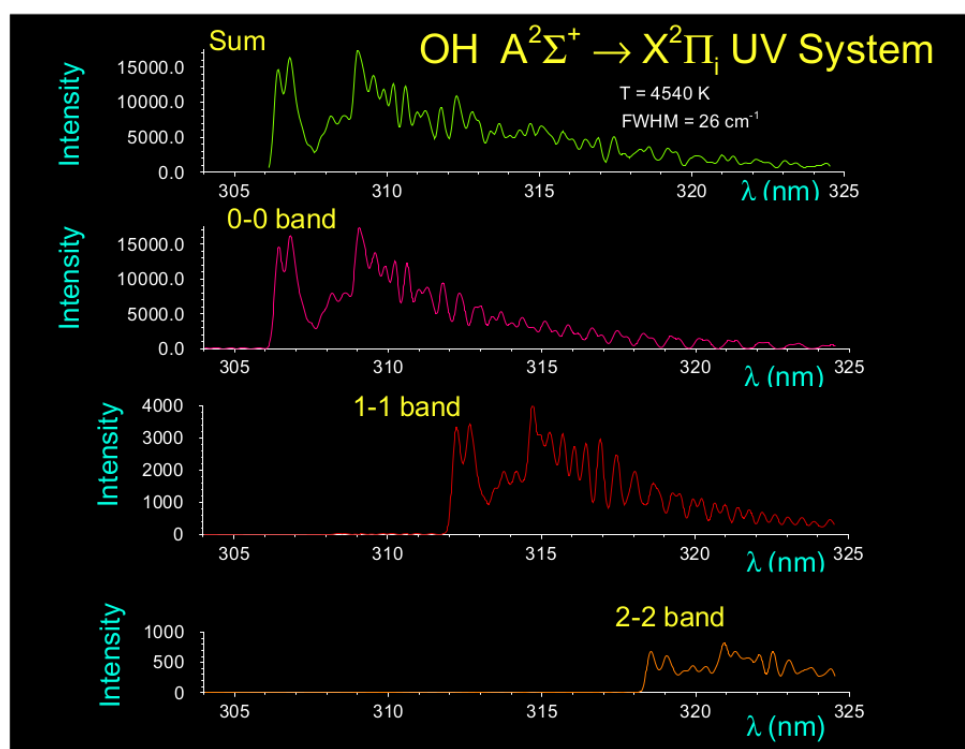


**Figure 6.** Comparisons of measured and recorded laser-plasma emission spectroscopy [99].

In view of the shadowgraphs reported in this work (see Figure 1), averages of well-developed fluid physics phenomena were recorded with linear diode arrays, viz. summing along the slit-height. It would appear reasonable to determine an association of spatially resolved spectra with the recorded expansion. However, simultaneous recording of shadowgraphs and spectra would be necessary for establishment of expansion characteristics following laser-induced breakdown in air. Such an association of shadowgraphs for time-delays of the order of 1  $\mu$ s has been reported recently using CN emission spectroscopy [91]. Radon inverse transforms or computed tomography would appear necessary, but possibly Abel inverse transforms may be sufficient as one realizes the symmetry of the vortex indicated in Fig. 1.



## 5. Conclusions

This work illustrated analysis of recorded time-resolved OH spectra using accurate line strength files. Presence of the hydroxyl radical is usually associated with combustion, however in laboratory air that contains residual moisture, OH emissions occur as a result of recombination radiation. Laser-plasma and laser-induced fluorescence measurements indicate the accuracy of the OH line strength data that are made publicly available for the first time in this publication. Hydroxyl ultraviolet system line strengths complement those for aluminum monoxide, cyanide, diatomic carbon, and titanium monoxide already available for selected electronic transitions. Future work should address association of OH signals with spatial variations due to vortex-formation and implosions that can be visualized by employing effectively high shutter-speed shadowgraph photography that is limited by the pulse-width of the back light. The presented work is applicable to electrical-spark analytical chemistry. Moreover, comparisons of PGOPHER and of the nonlinear NMT predictions should be content of future research, including comparisons with LIFBASE predictions. These comparisons are expected to lead to further insights in analysis of laboratory laser-plasma and on an astronomical scale help advancements in exo-planet and interstellar-medium research.

**Author Contributions:** All authors contributed equally to this work.

**Funding:** This research received no external funding.

**Acknowledgments:** The authors wish to acknowledge the support in part by the Center for Laser Applications at the University of Tennessee Space Institute.

**Conflicts of Interest:** The authors declare no conflict of interest.

## Appendix A Hydroxyl line strengths

### Appendix A.1 Overview

The appendix communicates the hydroxyl line strengths for fitting of measured and computed spectra for the OH ultraviolet bands. The line-strength data for the ultraviolet system of OH are attached in a supplementary file, *OHuv-lsf.txt*. The details for the establishment of the line-strength data are communicated in the recently published book on diatomic molecular spectroscopy [9]. The line strength data can be utilized together with the previously published Nelder-Mead temperature (NMT) and Boltzman equilibrium spectroscopic temperature (BESP) [10] programs along with descriptions of how to use it. In other words, ultraviolet OH line strengths are added to the files for CN, AlO, C<sub>2</sub>, and TiO [10].

### Appendix A.2 Example data file and fitted spectra

This section summarizes typical fitting steps, and it includes recorded and fitted data for spectra presented in Section 4. The fitting routine has been applied previously laser-induced spectroscopy [5]. Hydroxyl recombination spectra occur subsequent to laser-induced optical breakdown in laboratory air. The analysis and interpretation of OH emission spectra is discussed in view of chemical equilibrium predictions [5]. Figure A1 shows recorded and re-fitted OH spectra together with the residual- or difference- spectrum.

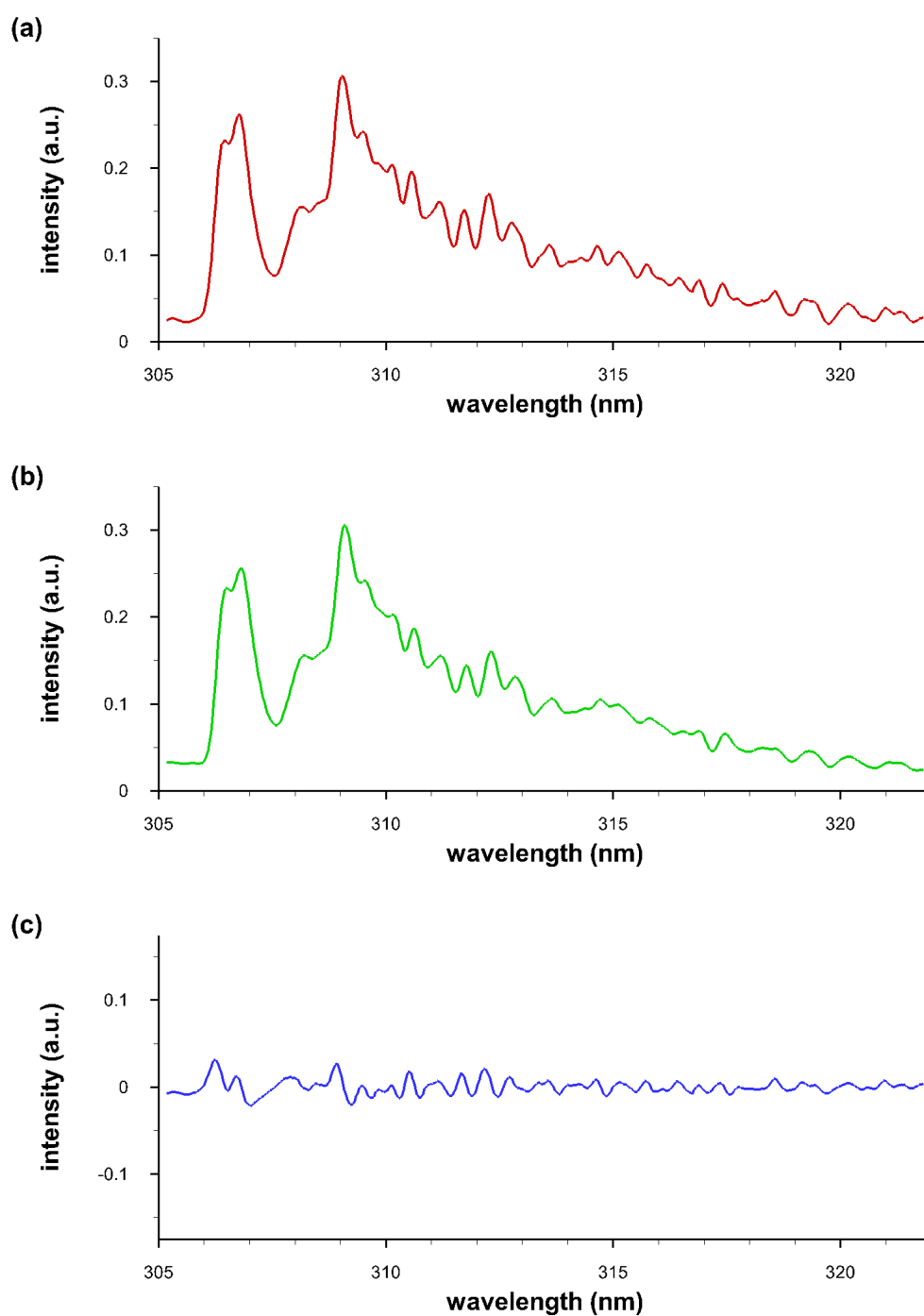


**Figure A1.** (a) Recorded and (b) fitted OH spectra. (c) Difference of measured and of fitted spectra. Time delay: 100  $\mu$ s, gate width: 50  $\mu$ s, temperature: 3,470 K.

The recorded and fitted data set comprised of 512 points of recorded signal versus calibrated wavelength are included as supplementary files "OH100micros.dat" and "OH100micros-fit.txt". The fitting results utilize a second-order polynomial for fitting background variation, temperature, and spectral line width. The inferred temperature equals  $T = 3,470$  K and the fitted line width,  $\Delta\lambda$ , equals  $\Delta\lambda = 0.36$  nm.

## References

- Kunze, H.-J. *Introduction to Plasma Spectroscopy*, Springer, Heidelberg, GER, 2009.
- Fujimoto, T. *Plasma Spectroscopy*, Clarendon Press, Oxford, UK, 2004.
- Ochkin, V.N. *Spectroscopy of Low Temperature Plasma*, Wiley-VCH, Weinheim, GER, 2009.
- Boulos, M.I.; Fauchais, P.; Pfender E. *Thermal Plasmas, Fundamentals and Applications*, Plenum Press, London, UK, 1994.
- Parigger, C.G.; Guan, G.; Hornkohl, J.O. Measurement and analysis of OH emission spectra following laser-induced optical breakdown in air. *Appl. Opt.* **2003**, *42*, 5986–5991.
- Parigger, C.G. Laser-induced breakdown in gases: Experiments and simulation. In *Laser Induced Breakdown Spectroscopy (LIBS): Fundamentals and Applications*; Miziolek, A.W., Palleschi, V., Schechter, I., Eds.; Cambridge Univ. Press: New York, NY, USA, 2006; pp. 171–193.
- Chen Y.-L.; Lewis, J.W.L. Visualization of laser-induced breakdown and ignition. *Opt. Express* **2001**, *9*, 360–372.
- Qin, W.; Chen, Y.-L.; Lewis, J.W.L. Time-resolved temperature images of laser-ignition using OH two-line laser-induced fluorescence (LIF) thermometry. *IFRF Combust. J.* **2005**, ISSN: 1562-479X, 200508.
- Parigger, C.G.; Hornkohl, J.O. *Quantum Mechanics of the Diatomic Molecule with Applications*, IOP Publishing, Bristol, UK, 2019.
- Parigger, C.G.; Woods, A.C.; Surmick, D.M.; Gautam, G.; Witte, M.J.; Hornkohl, J.O. Computation of diatomic molecular spectra for selected transitions of aluminum monoxide, cyanide, diatomic carbon, and titanium monoxide. *Spectrochim. Acta Part B: At. Spectrosc.* **2015**, *107*, 132–138.
- Luque, L.; Crosley, D.R. LIFBASE: Database and spectral simulation for diatomic molecules (Version 2.1.1). **2013**, <https://www.sri.com/cem/lifbase> (accessed on 3 September 2019).
- Parigger, C.G.; Surmick, D.M.; Helstern, C.M.; Gautam G.; Bol'shakov, A.A. Molecular Laser-Induced Breakdown Spectroscopy, In *Laser Induced Breakdown Spectroscopy, 2nd Ed.*; J.P. Singh, S.N. Thakur, Eds.; Elsevier New York, Amsterdam, NL, 2020; Chap. 7, in press.
- Yousefi, M.; Bernath P.F.; Hodges, J.; Masseron, T. A new line list for the  $A^2\Sigma^+ - X^2\Pi$  electronic transition of OH. *J. Quant. Spectrosc. Radiat. Transfer* **2018**, *217*, 416–424.
- Western, C.M. *J. Quant. Spectrosc. Radiat. Transf.* **2017**, *186*, 221–242.
- Tennyson, J. The ExoMol Project: Molecular Opacity Calculations at University College London, Workshop on Astrophysical Opacities, In: *Astronomical Society of the Pacific (ASP) Conference Series 515*, Michigan University, Kalamazoo, 1-4 August 2017, Michigan, US. Claudio Mendoza, Sylvaine Turck-Chi  ze, James Colgan (Eds.) *Astronomical Society of the Pacific* **2018**, 137.
- Tennyson, J.; Yurchenko, S.N.; Al-Refaie, A.F.; Barton, E.J.; Chubb, K.L.; Coles, P.A.; Diamantopoulou, S.; Gorman, M.N.; Hill, C.; Lam, A.Z.; Lodi, L.; McKemmish, L.K.; Na, Y.; Owens, A.; Polyansky, O.L.; Sousa-Silva, C.; Underwood, D.S.; Yachmenev, A.; Zak, E. The ExoMol database: Molecular line lists for exoplanet and other hot atmospheres. *arXiv* **2018**, [astro-ph.GA], 1603.05890 .
- Chernyak, V.Ya.; Nedybaliuk, O.A.; Martysh, E.V.; Iukhymenko, V.V.; Prysiashnevych, I.Y.; Solomenko, O.I.V.; Veremii, Iu.P.; Shevchenko, Taras. Low temperature plasma and plasma technologies: Plasmas catalysis of chemical reactions. *Prob. At. Sci. Technol. Ser.: Plasma Phys.* **2014**, *6*, 124–129.
- Srivastava, N.; Wang, C.J. Effect of N<sub>2</sub> and O<sub>2</sub> on OH radical production in an atmospheric helium microwave plasma jet. *Plasma Sci. Technol.* **2019**, *21*(11), 115401.
- Vora  , J.; Synek, P.; Proch  zka, V.; Hoder, T. State-by-state emission spectra fitting for non-equilibrium plasmas: OH spectra of surface barrier discharge at argon/water interface. *J. Phys. D - Appl. Phys.* **2017**, *50*(29), 294002.
- Ribarov, L.A.; Hu, S.; Wehrmeyer, J.A.; Pitz, W. Hydroxyl tagging velocimetry method optimization: signal intensity and spectroscopy. **2005**, *Appl. Opt.*, *44*(31), 6616–6626.
- Abrams, M. C.; Davis, S. P.; Rao, M. L. P.; Engleman, R. Jr.; Brault, J. W. High-resolution Fourier transform spectroscopy of the Meinel system of OH. *Astrophys. J., Suppl. Ser.* **1994**, *93*, 351–395.
- Stark, G., et al. Fourier-transform spectra of the  $A^2\Sigma^+ - X^2\Pi$   $\Delta v = 0$  bands of OH and OD. *J. Opt. Soc. Am. B - Opt. Phys.* **1994**, *11*(1), 3–32.
- Varberg, T. D.; Evenson, K.M. The rotational spectrum of OH in the  $v = 0-3$  levels of its ground-state. *J. Mol. Spectrosc.* **1993**, *157*(1), 55–67.

24. Becker, K.H.; Haaks, D.; Tatarczyk, T. The Natural lifetime of OH ( $^2\Sigma^+, v = 0, N = 2, J = 32$ ) and its quenching by atomic hydrogen. *Chem. Phys. Lett.* **1974**, *25*(4), 564–567.
25. Brockhinke, A.; Lenhard, U.; Bülter, A.; Kohse-Höinghaus, K. Energy transfer in the OH  $A^2\Sigma^+$  state: The role of polarization and of multi-quantum energy transfer. *Phys. Chem. Chem. Phys.* **2005**, *7*(5), 874–881.
26. Brophy, J. H.; Silver, J.A.; Kinsey, J.L. Direct measurement of the radiative lifetime of the  $A^2\Sigma^+(v' = 0, K' = 1, J' = 32)$  state of OH and OD. *Chem. Phys. Lett.* **1974**, *28*(3), 418–421.
27. Burris, J.; Butler, J.J.; McGee, T.J.; Heaps, W.S. Collisional deactivation rates for  $A^2\Sigma^+(v' = 1)$  state of OH. *Chem. Phys.* **1988**, *124*(2), 251–258.
28. Cattolica, R.J.; Mataga, T.G. (1991). Rotational-level-dependent quenching of OH  $A^2\Sigma^+(v' = 1)$  by collisions with  $H_2O$  in a low-pressure flame. *Chem. Phys. Lett.* **1991**, *182*(6), 623–631.
29. Cleveland, C.B.; Wiesenfeld, J.R. Electronic quenching of highly rotationally excited OH ( $A^2\Sigma^+, v' = 0, 1$ ) by  $H_2O$ . *Chem. Phys. Lett.* **1988**, *144*(5–6), 479–485.
30. Copeland, R.A.; Chalamala, B.R.; Coxon J.A. Laser-Induced Fluorescence of the  $B^2\Sigma^+ - X^2\Pi$  System of OH: Molecular constants for the  $B^2\Sigma^+(v = 0, 1)$  and  $X^2\Pi(v = 7 - 9, 11 - 3)$ . *J. Mol. Spectrosc.* **1993**, *161*(1), 243–252.
31. Copeland, R. A., Wiese, M.L, Crosley, D.R. Vibrational-Energy transfer and quenching of OH( $A^2\Sigma^+, v' = 1$ ). *J. Phys. Chem.* **1988**, *92*(20), 5710–5715.
32. Crosley, D. R.; Lengel, R.K. Relative transition-probabilities and electronic-transition moment in A-X system of OH. *J. Quant. Spectrosc. Radiat. Transfer* **1975**, *15*(7–8), 579–591.
33. Derro, E.L.; Pollack, I.B.; Dempsey, L.P.; Greenslade, M.F.; Lei, Y.; Radenović, D.Ć.; Lester, M.I. Fluorescence-dip infrared spectroscopy and predissociation dynamics of OH  $A^2\Sigma^+(v = 4)$  radicals. *J. Chem. Phys.* **2005**, *122*(24), 244313.
34. German, K.R. Direct measurement of radiative lifetime of  $A^2\Sigma^+(v' = 0)$  states of OH and OD. *J. Chem. Phys.* **1975**, *62*(7), 2584–2587.
35. German, K.R. Collision and quenching cross-sections in  $A^2\Sigma^+$  state of OH and OD. *J. Chem. Phys.* **1976**, *64*(10), 4065–4068.
36. Hogan, P.; Davis, D.D. Electronic quenching and vibrational-relaxation of OH ( $A^2\Sigma^+ v' = 1$ ) state - reply. *J. Chem. Phys.* **1976**, *64*(9), 3901–3901.
37. Hogan, P.; Davis, D.D. Electronic quenching and vibrational-relaxation of OH ( $A^2\Sigma^+ v' = 1$ ) state. *J. Chem. Phys.* **1975**, *62*(11) 4574–4576.
38. Huber, K.P.; Holland, F.; Coxon, J.A. Jet emission-spectroscopy of OH and OD near 1850-Å - 1st observation of  $A^2\Pi - ^2\Pi$  electronic-transition of OD. *J. Chem. Phys.* **1992**, *96*(2), 1005–1015.
39. Jorg, A.; Esposito, D.; Werner, H.J. Rotational energy-transfer in OH ( $A^2\Sigma^+, v' = 0$ ) - a method for the direct determination of state-to-state transfer-coefficients. *J. Chem. Phys.* **1990**, *93*(9), 6453–6462.
40. Kienle, R.; Li, M.P.; Kohse-Höinghaus, K. A detailed rate equation model for the simulation of energy transfer in OH laser-induced fluorescence. *Appl. Phys. B - Lasers Opt.* **1996**, *62*(6), 583–599.
41. McDermid, I.S.; Laudenslager, J.B. Radiative lifetime and quenching rate coefficients for directly excited rotational levels of OH ( $A^2\Sigma^+, v = 0$ ). *J. Chem. Phys.* **1982**, *76*(4), 1824–1831.
42. Rahmann, U.; Kreutner, W.; Kohse-Höinghaus, K. Rate-equation modeling of single- and multiple-quantum vibrational energy transfer of OH ( $A^2\Sigma^+, v' = 0$  to 3). *Appl. Phys. B - Lasers Opt.* **1999**, *69*(1), 61–70.
43. Bormann, F.C.; Nielsen, T.; Burrows, M.; Andresen, P. Single-pulse collision-insensitive picosecond planar laser-induced fluorescence of OH  $A^2\Sigma^+(v' = 2)$  in atmospheric-pressure flames. *Appl. Phys. B - Lasers Opt.* **1996**, *62*(6), 601–607.
44. Bormann, F.C.; Nielsen, T.; Burrows, M.; Andresen, P. Picosecond planar laser-induced fluorescence measurements of OH  $A^2\Sigma^+(v' = 2)$  lifetime and energy transfer in atmospheric pressure flames. *Appl. Opt.* **1997**, *36*(24), 6129–6140.
45. Brockhinke, A.; Kreutner, W.; Rahmann, U.; Kohse-Höinghaus, K.; Settersten, T.B.; Linne, M.A. Time-, wavelength-, and polarization-resolved measurements of OH ( $A^2\Sigma^+$ ) picosecond laser-induced fluorescence in atmospheric- pressure flames. *Appl. Phys. B - Lasers Opt.* **1999**, *69*, 477–485.
46. Brophy, J. H.; Silver, J.A.; Kinsey, J.L. Vibrationally excited OH from the reaction of H with  $NO_2$  observed by laser-induced fluorescence. *J. Chem. Phys.* **1975**, *62*(9), 3820–3822.
47. Cattolica, R. OH rotational temperature from 2-line laser-excited fluorescence. *Appl. Opt.* **1981**, *20*(7), 1156–1166.



48. Chen, H.; Hu, R.; Xie, P.; Xing, X.; Ling, L.; Li, Z.; Wang, F.; Wang, Y.; Liu, J.; Liu, W. A hydroxyl radical detection system using gas expansion and fast gating laser-induced fluorescence techniques. *J. Environ. Sci.* **2018**, *65*, 190–200.
49. Copeland, C.; Friedman, J.; Renksizbulut, M. (2007). "Planar temperature imaging using thermally assisted laser induced fluorescence of OH in a methane-air flame. *Exp. Therm. Fluid Sci.* **2007**, *31*(3), 221–236.
50. Crosley, D.R.; Smith, G.P. (1980). Vibrational energy-transfer in laser-excited  $A^2\Sigma^+$  OH as flame thermometer. *Appl. Opt.* **1980**, *19*(4), 517–520.
51. Dilecce, G.; Martini, L.M.; Cepelli, M.; Scotoni, M.; Tosi, P. Progress on laser induced fluorescence in a collisional environment: The case of OH molecules in ns pulsed discharges. *Plasma Sources Sci. Technol.* **2019**, *28*(2), 025012.
52. Dreizler, A.; Taday, R.; Monkhouse, P.; Wolfrum, J. Time and Spatially Resolved LIF of OH  $A^2\Sigma^+$  ( $v' = 1$ ) in Atmospheric-Pressure Flames using Picosecond Excitation. *Appl. Phys. B - Photophys. Laser Chem.* **1993**, *57*(1) 85–87.
53. Kienle, R.; Lee, M.P.; Kohse-Höinghaus, K. A scaling formalism for the representation of rotational energy transfer in OH ( $A(2)\Sigma^+$ ) in combustion experiments. *Appl. Phys. B - Lasers Opt.* **1996**, *63*(4), 403–418.
54. Killinger, D.K.; Hanabusa, M. Intensity and pressure-dependence of resonance fluorescence of OH induced by a tunable uv laser. *Phys. Rev. A* **1976**, *13*(6), 2145–2152.
55. Kollner, M.; Monkhouse, P. Time-resolved LIF of OH in the flame front of premixed and diffusion flames at atmospheric pressure. *Appl. Phys. B - Lasers Opt.* **1995**, *61*(5), 499–503.
56. Malmqvist, E.; Jonsson, M.; Larsson, K.; Aldén, M.; Bood, J. Two-dimensional OH-thermometry in reacting flows using photofragmentation laser-induced fluorescence. *Comb. Flame* **2016**, *169*, 297–306.
57. Mather, J.H.; Stevens, P.S.; Brune, W.H. OH and HO<sub>2</sub> measurements using laser-induced fluorescence. *J. Geophys. Res.: Atmos.* **1997**, *102*(D5), 6427–6436.
58. Nielsen, T.; Bormann, F.; Burrows, M.; Andresen, P. Picosecond laser-induced fluorescence measurement of rotational energy transfer of OH  $A^2\Sigma^+$  ( $v' = 2$ ) in atmospheric pressure flames. *Appl. Opt.* **1997**, *36*(30), 7960–7969.
59. Sappey, A.D.; Copeland, R.A. Laser double-resonance study of OH ( $X^2\Pi_i, v = 12$ ). *J. Mol. Spectrosc.* **1990**, *143*(1), 160–168.
60. Sick, V.; Wermuth, N. Single-shot imaging of OH radicals and simultaneous OH radical/acetone imaging with a tunable Nd:YAG laser. *Appl. Phys. B - Lasers Opt.* **2004**, *79*(2), 139–143.
61. Stone, D.; Whalley, L.K.; Ingham, T.; Edwards, P.M.; Cryer, D.R.; Brumby, C.A.; Seakins, P.W.; Heard, D.E. Measurement of OH reactivity by laser flash photolysis coupled with laser-induced fluorescence spectroscopy. *Atmos. Meas. Tech.* **2016**, *9*(7), 2827–2844.
62. Wang, F.; Hu, R.; Chen, H.; Xiew, P.; Wang, Y.; Li, Z.; Jin, H.; Liu, J.; Liu, W. Development of a field system for measurement of tropospheric OH radical using laser-induced fluorescence technique. *Opt. Expr.* **2019**, *27*(8), A419–A435.
63. Zizak, G.; Lanauze, J.A.; Winefordner, J.D. An experimental study of the excited state rotational population of OH in flames using laser induced fluorescence. *Combust. Flame* **1986**, *65*, 203–214.
64. Graña-Otero, J.; Mahmoudi, S. Excited OH kinetics and distribution in H<sub>2</sub> premixed flames. *Fuel* **2019**, *255*, 1115750.
65. Greenslade, M.E.; Letser, M.I. (2+1) resonance-enhanced ionization spectroscopy of a state-selected beam of OH radicals. *J. Chem. Phys.* **2005**, *123*(7), 074309.
66. Jeffries, J.B.; Kohse-Höinghaus, K.; Smith, G.P.; Copeland, R.A.; Crosley, D.R. Rotational-level-dependent quenching of OH( $A^2\Sigma^+$ ) at flame temperatures. *Chem. Phys. Lett.* **1988**, *152*(2-3), 160–166.
67. Kiefer, J.; Meyerhoefer, A.; Seeger, T.; Leipertz, A.; Li, Z.S.; Aldén, M. OH-thermometry using laser polarization spectroscopy and laser-induced fluorescence spectroscopy in the OH A-X (1,0) band. *J. Raman Spectrosc.* **2009**, *40*(7), 828–835.
68. Neuber, A. A.; Janicka, A.; Hassel, E.P. Thermally assisted fluorescence of laser-excited OH  $A^2\Sigma^+$  as a flame diagnostic tool. *Appl. Opt.* **1996**, *35*(21), 4033–4040.
69. Palmer, J.L.; Hanson, R.K. Temperature imaging in a supersonic free jet of combustion gases with two-line OH fluorescence. *Appl. Opt.* **1996**, *35*(3), 485–499.
70. Smith, G.P.; Crosley, D.R. Vibrational-energy transfer in  $A^2\Sigma^+$  OH in flames. *Appl. Opt.* **1983**, *22*(10), 1428–1430.

71. Wang, Y.; Jain, A.; Kulatilaka, W. Hydroxyl radical planar imaging in flames using femtosecond laser pulses. *Appl. Phys. B - Lasers Opt.* **2019**, *125*, 90.
72. Carlone, C.; Dalby, F. W. Spectrum of the hydroxyl radical. *Can. J. Phys.* **1969**, *47*(18), 1945–1957.
73. Copeland, R.A.; Jeffries J.B.; Crosley, D.R. The OH A  $^2\Sigma^+$  – X $^2\Pi_i$ (4,2) band-line positions and linewidths, *J. Mol. Spectrosc.* **1990**, *143*(1), 183–185.
74. Coxon, J.A.; Foster, S.C. Rotational analysis of hydroxyl vibration-rotation emission bands: Molecular constants for OH X $^2\Pi$ ,  $6 \leq v \leq 10$ . *Can. J. Phys.* **1980**, *60*, 41–48.
75. Coxon, J.A.; Sappey, A.D.; Copeland, R.A. Molecular constants and term values for the hydroxyl radical, OH: The X $^2\Pi$ ( $v=8,12$ ), A $^2\Sigma^+$ ( $v=4-9$ ), B $^2\Sigma^+$ ( $v=0,1$ ), and C $^2\Sigma^+$ ( $v=0,1$ ) states. *J. Mol. Spectrosc.* **1991**, *145*, 41–55.
76. Dieke, G.H.; Crosswhite, H.M. The ultraviolet bands of OH - fundamental data. *J. Quant. Spectrosc. Radiat. Transfer* **1962**, *2*, 97–199.
77. Dyer, M.J.; Knutsen, K.; Copeland, R.A. Energy transfer in the ground state of OH: Measurements of OH( $v = 8, 10, 11$ ) removal. *J. Chem. Phys.* **1997**, *107*(19), 7809–7815.
78. Gillis, J.R.; Goldman, A.; Stark, G.; Rinsland, C.P. Line parameters for the A  $^2\Sigma^+$  – X $^2\Pi$  bands of OH. *J. Quant. Spectrosc. Radiat. Transfer* **2001**, *68*(2), 225–230.
79. Hwang, E.S.; Lipson, J.B.; Field, R.W.; Dood, J.R. Detection of OH ( $X, v'', J''$ ) via the B  $^2\Sigma^+$  – X $^2\Pi$  transition and properties of the B  $^2\Sigma^+$  state." *J. Phys. Chem. A* **2001**, *105*(25), 6030–6037.
80. Langhoff, S.R.; Partridge, H. Theoretical-study of the lambda-doubling parameters for X  $^2\Pi$  OH. *J. Mol. Spectrosc.* **1984**, *105*(2) 261–275.
81. Langhoff, S.R.; Sink, M.L.; Pritchard, R.H.; Kern, C.W. Theoretical-study of the spin-orbit coupling in the X $^2\Pi$  state of OH. *J. Mol. Spectrosc.* **1982**, *96*(1), 200–218.
82. Lengel, R.K.; Crosley, D.R. Rotational dependence of vibrational-relaxation in A  $^2\Sigma^+$  OH. *Chem. Phys. Lett.* **1975**, *32*(2), 261–264.
83. Lengel, R.K.; Crosley, D.R. Electronic quenching and vibrational-relaxation of OH(A  $^2\Sigma^+$ ,  $v' = 1$ ) state - reply. *J. Chem. Phys.* **1976**, *64*(9), 3900–3901.
84. Lengel, R.K.; Crosley, D.R. Energy-transfer in  $^2\Sigma^+$  OH I. Rotational. *J. Chem. Phys.* **1977**, *67*(5), 2085–2101.
85. Lengel, R.K.; Crosley, D.R. Energy-transfer in  $^2\Sigma^+$  OH II. Vibrational. *J. Chem. Phys.* **1978**, *68*(12), 5309–5324.
86. Levin, D. A.; Laux, C.O.; Kruger, C.H. A general model for the spectral calculation of OH radiation in the ultraviolet. *J. Quant. Spectrosc. Radiat. Transfer* **1999**, *61*(3), 377–392.
87. Lucht, R.P.; Sweeney, D.W.; Laurendeau, N.M. Time-resolved fluorescence investigation of rotational transfer in A  $^2\Sigma^+$  ( $v = 0$ ) OH. *Appl. Opt.* **1986**, *25*(22), 4086–4095.
88. Raab, F.; Bergeman, T.; Lieberman, D.; Metcalf, H. Precision study of the A  $^2\Sigma^+$  state of the OH radical. *Phys. Rev. A* **1981**, *24*(6), 3120–3135.
89. Sechler, T.D.; Dempsey, L.O.; Lester, M.I. State-to-State Vibrational Energy Transfer in OH A  $^2\Sigma^+$  with N $_2$ . *J. Phys. Chem. A* **2009**, *113*(31), 8845–8851.
90. Steffens, K. L.; Crosley, D.R. Vibrational energy transfer in OH A  $^2\Sigma^+$  between 195 and 295 K. *J. Chem. Phys.* **2000**, *112*(21), 9427–9432.
91. Parigger, C.G.; Helstern, C.M.; Jordan, B.S.; Surmick, D.M.; Splinter, R. Laser-Plasma Spatiotemporal Cyanide Spectroscopy and Applications. *Molecules* **2020**, *25*, 615.
92. Cremers, D.A.; Radziemski, L.J. Handbook of Laser-Induced Breakdown Spectroscopy, John Wiley & Sons Ltd., USA, 2006.
93. Singh, J.P.; Thakur, S.N. (Eds.) Laser Induced Breakdown Spectroscopy, Elsevier Science, New York, USA, 2007.
94. Gautam, G.; Helstern, C.M.; Drake, K.A.; Parigger, C.G. Imaging of Laser-induced Plasma Expansion Dynamics in Ambient Air. *Int. Rev. At. Mol. Phys.* **2016**, *7*, 45–51.
95. Brieschenk, S.; O'Byrne, S.; Kleine, H. Visualization of jet development in laser-induced plasmas. *Opt. Lett.* **2013**, *38*(5), 664–666.
96. Harilal, S.S.; Miloshevsky, G.V.; K. Diwakar, LaHaye, N., Hassanein, A. Experimental and computational study of complex shockwave dynamics in laser ablation plumes in argon atmosphere. *Phys. Plasmas* **2012**, *19*, 083504.
97. Guan, G. On the analysis of emission spectra and interference images. Ph.D. dissertation (University of Tennessee, Knoxville, Tenn., 1998).

98. Parigger, C.G.; Guan, G.; Hornkohl, J.O. Laser-induced breakdown spectroscopy: analysis of OH spectra. In *Laser Induced Plasma Spectroscopy and Applications*; Vol. 81 of *Trends in Optics and Photonics Series*, Optical Society of America, Washington, DC, USA, 2002; pp. 102–103.
99. Hornkohl, J.O. Private communication (19 January 1996).